Nanoscale

COMMUNICATION

View Article Online
View Journal | View Issue

Cite this: *Nanoscale*, 2025, **17**, 12065

Received 6th January 2025,
Accepted 3rd March 2025

DOI: 10.1039/d5nr00050e

rsc.li/nanoscale

Robust large-area molecular junctions of self-assembled monolayers of a model helical paddlewheel complex†

Isabel Coloma,[a] Thierry Buffeteau,[b] Gilles Pecastaings,[c] Santiago Herrero,[a,d] Elizabeth Hillard,[e] Patrick Rosa,[e] Miguel Cortijo *[a] and Mathieu Gonidec *[e]

We report the preparation of a helical complex and its study in molecular junctions. We show that the SAMs of this racemic compound present electrically robust behaviour which will pave the way for future studies on the CISS effect with analogous enantiopure compounds.

Introduction

In recent years, there has been growing interest in the study of charge transport in chiral media. In particular, it has been shown that the current density across molecular junctions embedding chiral compounds and ferromagnetic electrodes can exhibit a great spin selectivity, which translates into strongly asymmetric *J*/V characteristics that critically depend on both the direction of magnetization of the electrode and the handedness of the chiral medium.[1,2] This effect is just one of many manifestations of a phenomenon discovered rather recently, termed the chirality-induced spin selectivity (CISS) effect. Since its discovery in photoelectron scattering experiments in 1999,[3] it has been the focus of intense experimental and theoretical efforts[4–6] and has now been observed in a great variety of physical systems, most typically using self-assembled monolayers of chiral molecular systems.[7] To this day, however, it remains highly challenging to predict the magnitude or even the occurrence of the CISS effect in new chiral molecular systems, which is due both to the limited availability of comparable experimental data sets and to the poor correlation between theoretical predictions and actual experimental results, often disagreeing by many orders of magnitude. With this in mind, it is crucial to support theoretical work by developing new platforms for the study of the CISS effect in molecular systems that are versatile and can be tuned rather easily. In this regard, we firmly believe that coordination chemistry provides interesting avenues for the study of the CISS effect since it allows for an unparalleled ad-hoc tuning of the electronic properties of the compounds – by changing the core metal ions – while maintaining the organic ligands, and thus, the overall geometry of the compounds is almost unchanged. While there are some examples of coordination compounds and metallopeptides that have been studied for the CISS effect,[8,9] the family of linear coordination clusters called the extended metal atom chains (EMACs)[10] would constitute a particularly appealing target for CISS studies. They include chains of up to 11 metal ions[11] and possess an optical activity that rivals that of the best helicenes.[12,13] Their chemistry, however, is somewhat challenging and the analogous, simpler, paddlewheel metal–metal bonded binuclear ruthenium compounds represent an interesting starting point, owing to their chemical stability and to their rather high spin moment. They have been considerably studied in the last few decades because of their potential applications in fields such as magnetism,[14–16] molecular electronics,[17–19] biomedicine,[20–28] and catalysis.[29–32] Most diruthenium complexes contain a Ru_2^{5+} core supported by four monoanionic equatorial bridging ligands and one or two axial ligands. The most common electronic configuration of these compounds is $\sigma^2\pi^4\delta^2(\pi^*\delta^*)^3$, with three unpaired electrons in the nearly degenerate π* and δ* molecular orbitals and a metal–metal bond order of 2.5.[33] Among diruthenium compounds, $[Ru_2(\mu\text{-ap})_4Cl]$ (RuapCl; ap = 2-anilinopyridinate), with four unsymmetrical ap ligands in the same orientation (4,0 isomer), was first reported a few decades ago.[34] This compound and its related derivatives have been studied mainly because of their isomerism and the effects of different axial

[a]*MatMoPol Research Group, Department of Inorganic Chemistry, Faculty of Chemical Sciences, Complutense University of Madrid, Avda. Complutense s/n, 28040 Madrid, Spain. E-mail: miguelcortijomontes@ucm.es*
[b]*Univ. Bordeaux, CNRS, Bordeaux INP, ISM, UMR 5255, F-33405 Talence, France*
[c]*Univ. Bordeaux, CNRS, CRPP, UMR 5031, F-33600 Pessac, France*
[d]*Knowledge Technology Institute, Complutense University of Madrid, Campus de Somosaguas, 28223 Pozuelo de Alarcón, Madrid, Spain*
[e]*Univ. Bordeaux, CNRS, Bordeaux INP, ICMCB, UMR 5026, F-33600 Pessac, France. E-mail: mathieu.gonidec@icmcb.cnrs.fr*

†Electronic supplementary information (ESI) available: Experimental details, FTIR, UV-vis, magnetic susceptibility, additional AFM and ToF-SIMS data. See DOI: https://doi.org/10.1039/d5nr00050e

ligands or electron-withdrawing/donating substituents on their electronic properties.[35–43] Moreover, the study of electronic transport properties of acetylide derivatives has been a subject of interest. More specifically, the electronic transport properties of $[Ru_2(\mu\text{-ap})_4(\sigma\text{-}(C{\equiv}CC_6H_4)_2SCH_2CH_2SiMe_3)]$ embedded in a C_{11} thiol matrix on a gold substrate[17] and self-assembled $[Ru_2(\mu\text{-ap})_4(\sigma\text{-}(C{\equiv}CC_6H_4)_2S{-})_2]$ and $[Ru_2(\mu\text{-ap})_4(\sigma\text{-}C{\equiv}CC_6H_4S{-})]$ fragments in nanogap molecular junctions[18] were reported by Ren and coworkers.

A relatively unexplored feature of the $[Ru_2(\mu\text{-ap})_4]^+$ scaffold – one that is particularly interesting for the CISS effect – is its helical chirality, which arises from the arrangement of the 2-anilinopyridinate ligands around the ruthenium atoms generating two enantiomers, Δ (clockwise helicity) and Λ (counter-clockwise helicity). However, in order to use such compounds in chiral molecular junctions for the study of the CISS effect it is necessary to develop a robust methodology for their deposition as stable self-assembled monolayers (SAMs) on surfaces. Ideally, this methodology should be transferable to EMACs and should provide electrically robust systems with a narrow statistical distribution of current density values in order to be able to determine the magnitude of the CISS effect with good statistical significance. The classical methodologies for making SAMs based on alkanethiol tethers are challenging to implement for such compounds and would not allow the helical axis of the compounds to align normally to the surface, which would be ideal for studying the CISS effect. In this paper, we study a covalent grafting strategy for anchoring a racemic mixture of a model diruthenium complex. We use the easy and common strategy of substituting the axial ligand (typically a halide) with an –NCS thiocyanate ligand and show that it forms well-defined smooth monolayers on template-stripped gold substrates (Au^{TS}). We also show that the molecular junctions formed by these monolayers coming in contact with a eutectic gallium–indium (EGaIn) tip are electrically robust with a narrow distribution of current density values. Altogether, these results on a racemic system demonstrate that this methodology – once applied to enantiopure compounds – provides a promising platform for studying the CISS effect in large-area junctions of paddlewheel complexes, which could be extended to EMACs and coordination compounds in general.

Results and discussion

Synthesis and characterization of $[Ru_2(\mu\text{-ap})_4(NCS)]$ (RuapNCS)

In this study, we chose to target a rather simple racemic dinuclear paddlewheel complex bearing an isothiocyanate group, whose protruding sulfur atom was expected to provide an anchoring group for the surface chemistry, as has been shown in a few examples for single-molecule junctions in EMACs and other coordination complexes.[44–46] We started from a well-known racemic, helicoidal (see Fig. S1†) diruthenium compound, **RuapCl**, developed by the Cotton group in the early 80s.[34] The complex **RuapNCS** was prepared in one step by reacting a slight excess of KSCN with the chloride analogue **RuapCl** (see Scheme 1). The mixture was filtered to remove the resulting KCl and a dichloromethane/water liquid/liquid extraction was carried out to remove the remaining KSCN.

The bulk sample was characterized by elemental analysis, mass spectrometry, infrared and electronic spectroscopy, and variable-temperature magnetic susceptibility measurements.

The base peak of the positive electrospray ionization (ESI^+) mass spectrum of most Ru_2^{5+} complexes corresponds to the $[M - X]^+$ fragment, resulting from the loss of the axial ligand (X).[26] However, the base peak observed for the spectrum of **RuapNCS** corresponds to $[M]^+$ (m/z = 937.97). The experimental isotopic pattern of this $[M]^+$ fragment matches perfectly with the calculated one (see Fig. 1), confirming the nature of the desired product. The presence of this $[M]^+$ fragment and the absence of $[M - NCS]^+$ suggest a greater stability of the complex given a stronger Ru–L_{axial} bond compared to other closely related compounds.[38,47]

Infrared spectroscopy also confirms the isolation of a monodentate isothiocyanate derivative, since a strong –N═C═S asymmetric stretching band is observed at 2034 cm^{-1} (Fig. S2†).[48] This relatively low value also suggests a strong Ru–N bond due to π back-bonding. The electronic structure of the new complex was studied by UV/vis-NIR spectroscopy. Fig. S3† shows the electronic spectrum in which four bands can be distinguished. Regarding the ultraviolet region, two absorption bands are observed at ~275 and ~325 nm, which can be assigned to an intra-ligand π → π* transition and a π(N)/δ*(Ru_2) → π*(aryl) transition, respectively. In the visible

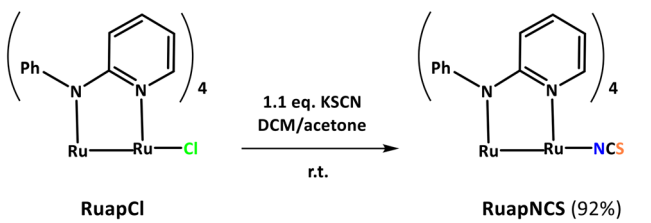

RuapCl **RuapNCS** (92%)

Scheme 1 One-step synthesis of **RuapNCS** from the chloride analogue **RuapCl**.

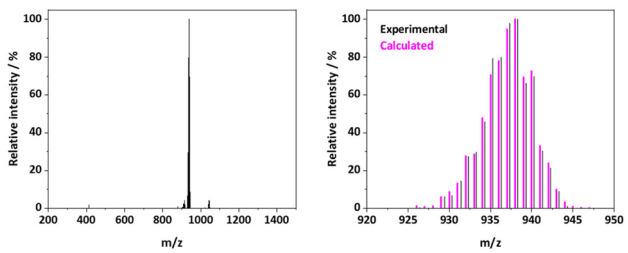

Fig. 1 ESI^+ spectra (left) and enlargement of the $[M]^+$ base peak (right) of **RuapNCS**.

range, two more bands are recorded at ~465 and 770 nm. The first one can be assigned mainly to $\pi(Ru_2) \rightarrow \pi^*(N)/\delta^*(Ru_2)$ and the second one to $\pi(Ru\text{–}N) \rightarrow \delta^*(Ru_2)$.[43] Table S1† lists these absorption bands and their assignments.

The variable temperature magnetization measurements performed on **RuapNCS** showed a $\chi_M T$ value at room temperature of 1.83 cm^3 K mol^{-1}, slightly lower than the spin-only value expected from a quartet state (1.87 cm^3 K mol^{-1}, g = 2). Lowering the temperature results in a continuous decrease of the $\chi_M T$ product, which is especially pronounced below 100 K. The data were fitted considering a quartet state, which arises from a $\sigma^2\delta^2\pi^4(\delta^*\pi^*)^3$ electronic configuration, undergoing axial zero-field splitting (D). In addition, an intermolecular exchange coupling (zJ) was included in the model using the mean-field approximation (Fig. S4 and eqn (S1)–(S4)†). The following parameters were obtained from the best fit to the data: g = 1.997(1), D = 45.0(7) cm^{-1} and zJ = −0.11(1) cm^{-1} (σ^2 = 3.00 × 10^{-4}). These values are similar to those reported for closely related complexes[43,49–51] and discard the low spin configuration found in other Ru_2^{5+} derivatives with a thiocyanate ligand at the axial position.[47]

Preparation and characterization of Au^{TS}–RuapNCS/Au–RuapNCS

Once **RuapNCS** was fully characterized, self-assembled monolayers (SAMs) were prepared by incubating template-stripped gold (for AFM and EGaIn measurements) or standard gold (for ToF-SIMS and PM-IRRAS measurements) substrates in toluene solutions at room temperature using classical wet chemistry methods. Control samples were prepared with the same protocol using **RuapCl**. The monolayers, Au^{TS}–**RuapNCS**, and the control samples, Au^{TS}–**RuapCl**, were then studied by a combination of atomic force microscopy (AFM), time of flight secondary ion mass spectrometry (ToF-SIMS) and polarization-modulation infrared reflection absorption spectroscopy (PM-IRRAS).

The morphology of the Au^{TS}–**RuapNCS** substrate after 3.5 h of incubation was probed by AFM in tapping mode and was shown to be extremely smooth (see Fig. 2). The roughness of the monolayer was found to be similar to that of the blank Au^{TS} substrate (see Fig. S5†), with rms values of 2.6 and 2.9 Å, respectively. The main difference between the two samples appeared to be a smaller number of particles on the surface of the monolayer and the disappearance of the grain boundaries of the underlying gold substrate in the SAMs. The AFM topography image for the control sample Au^{TS}–**RuapCl** (see Fig. S5†) was visually similar to that of the Au^{TS}–**RuapNCS** sample and presented a similar roughness to that of the other samples, with an rms value of 3.0 Å.

ToF-SIMS was performed in both negative and positive modes for substrates incubated in **RuapNCS** and **RuapCl** solutions. The spectra recorded for the Au–**RuapNCS** sample show several Au clusters and three peaks related to the complex can clearly be identified (Fig. 3a and S6†) thanks to their rather unique isotopic distribution while the negative mode was found to be not very informative (Fig. S6†). In particular, in the positive mode, fragments corresponding to $[M - NCS]^+$ are observed at m/z = 880.03. Besides, a minor contribution from the molecular peak is observed at m/z = 939.18, which can be assigned to $[M + H]^+$. Altogether, these results suggest the formation of self-assembled monolayers of the complex **RuapNCS** over template-stripped gold (Au^{TS}–**RuapNCS**), where **RuapNCS** molecules are anchored to the substrate through the isothiocyanate axial ligand. Moreover, a two-dimensional mapping analysis of the main peak was performed and the resulting ToF-SIMS image is shown in Fig. 3b. These 2D ToF-SIMS results show good homogeneity of the samples with a rather constant signal across the substrate and no significant local concentration of species that could result from aggregates. The

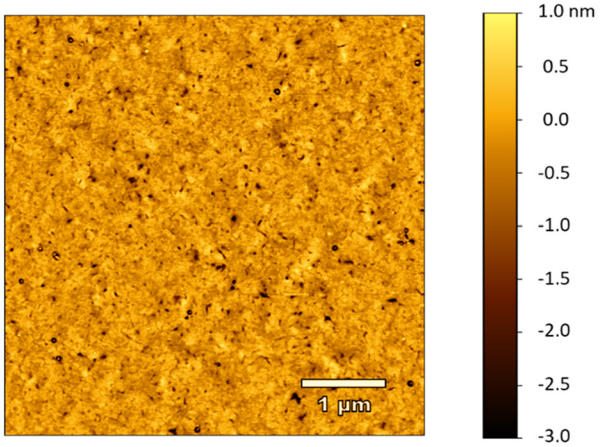

Fig. 2 Tapping-mode AFM topography image for Au^{TS}–**RuapNCS**.

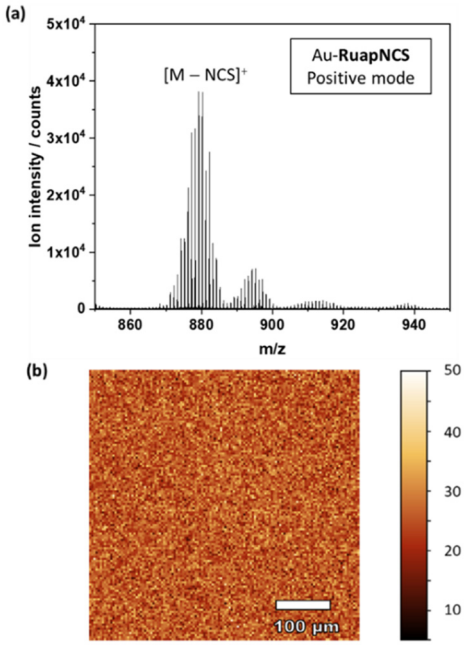

Fig. 3 (a) ToF-SIMS spectrum of ions derived from Au–**RuapNCS** in the positive mode. (b) 2D ToF-SIMS mapping for $[M - SCN]^+$ ions.

ToF-SIMS positive spectrum for the control sample Au–**RuapCl** (see Fig. S7†) also showed a prominent $[M - X]^+$ fragment but its intensity was reduced by a factor of approximately 3 with respect to the Au–**RuapNCS** monolayer sample (see Fig. S8†). This result likely indicates the presence of some physisorbed **RuapCl** molecules on the gold surface, with the amount likely depending on the amount of solvent used during the rinsing procedure.

The PM-IRRAS spectra recorded for the Au–**RuapNCS** (Fig. 4) and Au–**RuapCl** (Fig. S9†) samples mainly show the same bands as observed in the IR spectrum of the bulk compounds. Importantly, for Au–**RuapNCS**, a clear shift in the –N=C=S asymmetric stretching band can be observed, which is due to the anchoring of the complex to the substrate through the sulfur atom. The band is shifted from 2034 cm^{-1} to 2083 cm^{-1}, a variation that is consistent with an NCS bridging ligand (Au–SCN–Ru).[48] Moreover, as expected based on the selection rules of PM-IRRAS, there is a clear effect of the orientation of the molecules on the surface in the PM-IRRAS spectrum with respect to the isotropic ATR spectrum. Some bands are essentially suppressed while others are enhanced. These bands were assigned (Fig. S10†) on the basis of DFT calculations on the isolated molecule at the B3LYP/LANL2DZ level. The –N=C=S asymmetric stretching band is clearly intense, supporting the attachment of the molecule *via* the sulfur and aligned with the S=C=N–Ru–Ru direction normal to the substrate.

The pyridine ring (C=C and C=N) stretching band at 1540 cm^{-1} which has a transition dipole along the Ru–Ru direction (Fig. S11†) is also clearly enhanced. In contrast, the pyridine in-plane CH deformation and phenyl in-plane CH deformation bands at 1284 and 1215 cm^{-1} (Fig. S11†), respectively, that both correspond to transverse modes, are strongly suppressed in the PM-IRRAS spectrum. Altogether, this analysis confirms that the molecules are grafted on the surface *via* the sulfur atom with the Ru–Ru bond essentially normal to the surface.

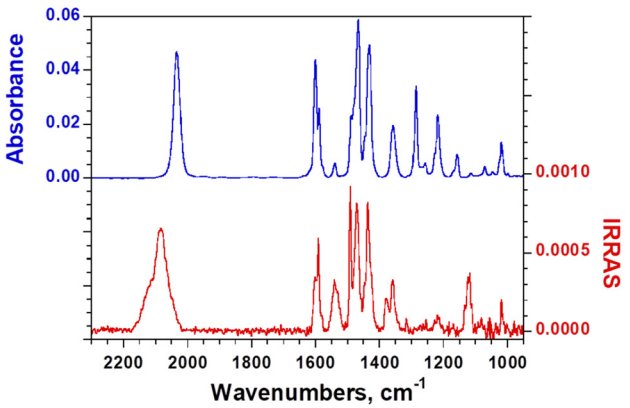

Fig. 4 Comparison between the bulk FTIR-ATR spectrum for RuapNCS and the PM-IRRAS spectrum for Au–RuapNCS.

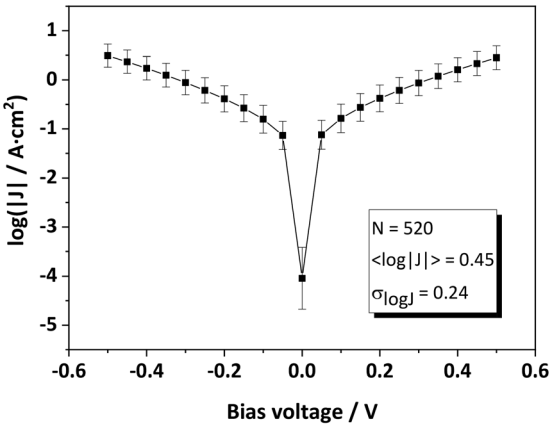

Fig. 5 Plot of <log(|*J*|)> *versus* applied bias voltage (V) for Au^{TS}–**RuapNCS**//Ga_2O_3/EGaIn junctions. The error bars correspond to the standard deviation.

Au^{TS}–RuapNCS//Ga_2O_3/EGaIn molecular junctions

In order to evaluate the robustness of the monolayers with respect to charge transport measurements, we then studied the Au^{TS}–**RuapNCS** SAMs using eutectic gallium–indium (EGaIn) top electrodes by using the classical conical tip method at room temperature. The resulting Au^{TS}–SAM//Ga_2O_3/EGaIn large-area junctions were measured in the ±0.5 V range. To obtain statistically robust data, we measured 14 junctions and accumulated 520 traces. The results are shown in Fig. 5. The junction yield was excellent; in fact, we did not observe a single short in the 14 junctions, and there were no significant outliers in the dataset.

The current density values were also found to be very robust and repeatable, with an average value of $\log(|J/\text{A cm}^{-2}|) = 0.45 \pm 0.24$ ($N = 520$) at 0.5 V; the standard deviation is essentially as good as that seen for model SAMs of *n*-alkanethiols[52] and the current density histogram presents a well-defined normal distribution (see Fig. S12†). There is no significant rectification in these junctions, which is not surprising given the molecular structure of the compounds, and this is consistent with the fact that the highest occupied molecular orbitals (as calculated by DFT, see Fig. S13†) are essentially delocalized over the whole complex. Moreover, the current density at 0.5 V ($\log|J| = 0.45$) is of the same order of magnitude as that observed for oligophenyl-methanethiol SAMs of similar length.[53] For the sake of comparison, we also attempted to measure molecular junctions of a control sample of Au^{TS}–**RuapCl**. However, as expected, the stability and/or quality of the physisorbed layer was too poor to allow measurement of its charge transport characteristics, and the EGaIn junctions invariably led to shorts.

Conclusions

We have shown here, with a model compound, that substituting linear coordination clusters with an axial isothiocyanate

ligand provides an interesting method for preparing monolayers in solution. These monolayers are both smooth and robust and can be easily incorporated into large-area molecular junctions whose electrical characteristics are outstanding. Specifically, the robustness of the SAMs allows for the measurement of EGaIn junctions without any shorts, and the distribution of current density values is as narrow as that of the best-performing organic SAMs. In this proof-of-concept study, we used a racemic mixture of a rather simple diruthenium paddlewheel complex. Although this racemic mixture is not directly relevant for the CISS effect because it contains an equal mixture of both enantiomers, the methodology applied here opens multiple avenues for future studies. In particular, in future work, we intend to resolve the enantiomers from the racemic mixture, which should yield enantiopure compounds that are expected to show a sizeable CISS effect. We will also study the possibility of spontaneous resolution on the surface using magnetic fields, which is a highly interesting prospect. Alternatively, we will synthesize and study closely related enantiopure analogues by using enantiopure chiral ligands, for which the strategy exposed herein will be directly applicable. Finally, this methodology will be applied to more complex coordination compounds such as EMACs which are expected to show an outstanding CISS effect due to their great optical activity.

Author contributions

M. G., I. C., E. H. and M. C. conceptualized the work. I. C. carried out the synthesis of the complex and I. C. and M. G. prepared the SAMs. The characterization of the bulk and the SAMs was performed by M. G., I. C., T. B. and G. P. for both data acquisition and curation. All authors participated in the formal analysis of the data. M. G., I. C. and M. C. drafted the original draft. All authors reviewed and edited the article. E. H., M. G. and S. H. secured the funding for this work.

Data availability

A selection of the experimental data was deposited in the French national open data repository recherche.data.gouv.fr (**https://dx.doi.org/10.57745/IN5TL6**).

Conflicts of interest

There are no conflicts to declare.

Acknowledgements

The authors acknowledge support from the Universidad Complutense de Madrid (GRFN32/23, GRFN24/24 and project PR3/23-30828), the France 2030 government investment plan managed by the French National Research Agency under grant reference PEPR SPIN – SPINMAT ANR-22-EXSP-0007, the Imperial College – CNRS joint PhD program, Quantum Matter Bordeaux, the MaelStroM project (CNRS MITI program), the National Research Agency project AnaCrU-CISS (ANR-23-CE09-0026) and the GPR Light project LIGHT-057-ChiroSurf.

I.C. acknowledges the predoctoral grant from the Complutense University of Madrid and Banco Santander (CT82/20-CT83/20). The authors warmly thank J.P. Salvetat of the Placamat service unit (France) for the ToF-SIMS measurements and Stéphane Toulin for assistance with the open data repository. Computer time for the theoretical calculation was provided by the computing facilities MCIA (Mésocentre de Calcul Intensif Aquitain) of the Université de Bordeaux.

References

1 F. Evers, A. Aharony, N. Bar-Gill, O. Entin-Wohlman, P. Hedegård, O. Hod, P. Jelinek, G. Kamieniarz, M. Lemeshko, K. Michaeli, V. Mujica, R. Naaman, Y. Paltiel, S. Refaely-Abramson, O. Tal, J. Thijssen, M. Thoss, J. M. van Ruitenbeek, L. Venkataraman, D. H. Waldeck, B. Yan and L. Kronik, *Adv. Mater.*, 2022, **34**, 2106629.
2 C. D. Aiello, J. M. Abendroth, M. Abbas, A. Afanasev, S. Agarwal, A. S. Banerjee, D. N. Beratan, J. N. Belling, B. Berche, A. Botana, J. R. Caram, G. L. Celardo, G. Cuniberti, A. Garcia-Etxarri, A. Dianat, I. Diez-Perez, Y. Guo, R. Gutierrez, C. Herrmann, J. Hihath, S. Kale, P. Kurian, Y. C. Lai, T. Liu, A. Lopez, E. Medina, V. Mujica, R. Naaman, M. Noormandipour, J. L. Palma, Y. Paltiel, W. Petuskey, J. C. Ribeiro-Silva, J. J. Saenz, E. J. G. Santos, M. Solyanik-Gorgone, V. J. Sorger, D. M. Stemer, J. M. Ugalde, A. Valdes-Curiel, S. Varela, D. H. Waldeck, M. R. Wasielewski, P. S. Weiss, H. Zacharias and Q. H. Wang, *ACS Nano*, 2022, **16**, 4989–5035.
3 K. Ray, S. P. Ananthavel, D. H. Waldeck and R. Naaman, *Science*, 1999, **283**, 814–816.
4 T. K. Das, F. Tassinari, R. Naaman and J. Fransson, *J. Phys. Chem. C*, 2022, **126**, 3257–3264.
5 Y. Dubi, *Chem. Sci.*, 2022, **13**, 10878–10883.
6 A. Chiesa, E. Garlatti, M. Mezzadri, L. Celada, R. Sessoli, M. R. Wasielewski, R. Bittl, P. Santini and S. Carretta, *Nano Lett.*, 2024, **24**, 12133–12139.
7 B. P. Bloom, Y. Paltiel, R. Naaman and D. H. Waldeck, *Chem. Rev.*, 2024, **124**, 1950–1991.
8 R. Torres-Cavanillas, G. Escorcia-Ariza, I. Brotons-Alcázar, R. Sanchis-Gual, P. C. Mondal, L. E. Rosaleny, S. Giménez-Santamarina, M. Sessolo, M. Galbiati, S. Tatay, A. Gaita-Ariño, A. Forment-Aliaga and S. Cardona-Serra, *J. Am. Chem. Soc.*, 2020, **142**, 17572–17580.
9 C. Wang, A.-M. Guo, Q.-F. Sun and Y. Yan, *J. Phys. Chem. Lett.*, 2021, **12**, 10262–10269.
10 J. F. Berry, in *Multiple Bonds Between Metal Atoms*, Springer US, Boston, MA, 2005, pp. 669–706.

11 P.-J. Chen, M. Sigrist, E.-C. Horng, G.-M. Lin, G.-H. Lee, C. Chen and S.-M. Peng, *Chem. Commun.*, 2017, **53**, 4673–4676.
12 D. W. Armstrong, F. A. Cotton, A. G. Petrovic, P. L. Polavarapu and M. M. Warnke, *Inorg. Chem.*, 2007, **46**, 1535–1537.
13 M. Cortijo, Á. Valentín–Pérez, P. Rosa, N. Daugey, T. Buffeteau and E. A. Hillard, *Chirality*, 2020, **32**, 753–764.
14 P. Angaridis, F. A. Cotton, C. A. Murillo, D. Villagrán and X. Wang, *J. Am. Chem. Soc.*, 2005, **127**, 5008–5009.
15 M. C. Barral, S. Herrero, R. Jiménez–Aparicio, M. R. Torres and F. A. Urbanos, *Angew. Chem., Int. Ed.*, 2005, **44**, 305–307.
16 G. M. Chiarella, F. A. Cotton, C. A. Murillo, K. Ventura, D. Villagrán and X. Wang, *J. Am. Chem. Soc.*, 2014, **136**, 9580–9589.
17 A. S. Blum, T. Ren, D. A. Parish, S. A. Trammell, M. H. Moore, J. G. Kushmerick, G.-L. Xu, J. R. Deschamps, S. K. Pollack and R. Shashidhar, *J. Am. Chem. Soc.*, 2005, **127**, 10010–10011.
18 A. K. Mahapatro, J. Ying, T. Ren and D. B. Janes, *Nano Lett.*, 2008, **8**, 2131–2136.
19 L. Welte, R. González-Prieto, D. Olea, M. R. Torres, J. L. Priego, R. Jiménez-Aparicio, J. Gómez-Herrero and F. Zamora, *ACS Nano*, 2008, **2**, 2051–2056.
20 M. Benadiba, I. De, M. Costa, R. L. S. R. Santos, F. O. Serachi, D. De Oliveira Silva and A. Colquhoun, *J. Biol. Inorg. Chem.*, 2014, **19**, 1025–1035.
21 S. R. Alves Rico, A. Z. Abbasi, G. Ribeiro, T. Ahmed, X. Y. Wu and D. De Oliveira Silva, *Nanoscale*, 2017, **9**, 10701–10714.
22 S. R. Alves, A. Colquhoun, X. Y. Wu and D. De Oliveira Silva, *J. Inorg. Biochem.*, 2020, **205**, 110984.
23 I. Coloma, M. Cortijo, M. J. Mancheño, M. E. León-González, C. Gutierrez, B. Desvoyes and S. Herrero, *Inorg. Chem. Front.*, 2023, **10**, 4402–4413.
24 H.-U. Rehman, B. Fornaciari, S. R. Alves, A. Colquhoun and D. De Oliveira Silva, *J. Microencapsul.*, 2023, **40**, 549–565.
25 I. Coloma, J. Parrón-Ballesteros, M. Cortijo, C. Cuerva, J. Turnay and S. Herrero, *Inorg. Chem.*, 2024, **63**, 12870–12879.
26 I. Coloma, M. Cortijo, I. Fernández-Sánchez, J. Perles, J. L. Priego, C. Gutiérrez, R. Jiménez-Aparicio, B. Desvoyes and S. Herrero, *Inorg. Chem.*, 2020, **59**, 7779–7788.
27 S. La Manna, C. Di Natale, V. Panzetta, M. Leone, F. A. Mercurio, I. Cipollone, M. Monti, P. A. Netti, G. Ferraro, A. Terán, A. E. Sánchez-Peláez, S. Herrero, A. Merlino and D. Marasco, *Inorg. Chem.*, 2024, **63**, 564–575.
28 S. La Manna, V. Panzetta, C. Di Natale, I. Cipollone, M. Monti, P. A. Netti, A. Terán, A. E. Sánchez-Peláez, S. Herrero, A. Merlino and D. Marasco, *Inorg. Chem.*, 2024, **63**, 10001–10010.
29 T. Miyazawa, T. Suzuki, Y. Kumagai, K. Takizawa, T. Kikuchi, S. Kato, A. Onoda, T. Hayashi, Y. Kamei, F. Kamiyama, M. Anada, M. Kojima, T. Yoshino and S. Matsunaga, *Nat. Catal.*, 2020, **3**, 851–858.
30 K. Makino, Y. Kumagai, T. Yoshino, M. Kojima and S. Matsunaga, *Org. Lett.*, 2023, **25**, 3234–3238.
31 J. K. Sailer, J. C. Sharland, J. Bacsa, C. F. Harris, J. F. Berry, D. G. Musaev and H. M. L. Davies, *Organometallics*, 2023, **42**, 2122–2133.
32 M. J. Trenerry, C. M. Wallen, T. R. Brown, S. V. Park and J. F. Berry, *Nat. Chem.*, 2021, **13**, 1221–1227.
33 J. G. Norman, G. E. Renzoni and D. A. Case, *J. Am. Chem. Soc.*, 1979, **101**, 5256–5267.
34 A. R. Chakravarty, F. A. Cotton and D. A. Tocher, *Inorg. Chem.*, 1985, **24**, 172–177.
35 J. L. Bear, Y. Li, B. Han, E. Van Caemelbecke and K. M. Kadish, *Inorg. Chem.*, 1997, **36**, 5449–5456.
36 K. M. Kadish, L.-L. Wang, A. Thuriere, L. Giribabu, R. Garcia, E. Van Caemelbecke and J. L. Bear, *Inorg. Chem.*, 2003, **42**, 8309–8319.
37 K. M. Kadish, L.-L. Wang, A. Thuriere, E. Van Caemelbecke and J. L. Bear, *Inorg. Chem.*, 2003, **42**, 834–843.
38 M. Nguyen, T. Phan, E. V. Caemelbecke, X. Wei, J. L. Bear and K. M. Kadish, *Inorg. Chem.*, 2008, **47**, 4392–4400.
39 S. Su, X. Zhu, Y. Wen, L. Zhang, Y. Yang, C. Lin, X. Wu and T. Sheng, *Angew. Chem., Int. Ed.*, 2019, **58**, 15344–15348.
40 K. M. Kadish, T. D. Phan, L. Giribabu, J. Shao, L.-L. Wang, A. Thuriere, E. Van Caemelbecke and J. L. Bear, *Inorg. Chem.*, 2004, **43**, 1012–1020.
41 E. Van Caemelbecke, T. Phan, W. R. Osterloh and K. M. Kadish, *Coord. Chem. Rev.*, 2021, **434**, 213706.
42 M. D. Roy, M. J. Trenerry, B. Thakuri, S. N. MacMillan, M. D. Liptak, K. M. Lancaster and J. F. Berry, *Inorg. Chem.*, 2022, **61**, 3443–3457.
43 A. R. Corcos, M. D. Roy, M. M. Killian, S. Dillon, T. C. Brunold and J. F. Berry, *Inorg. Chem.*, 2017, **56**, 14662–14670.
44 A. C. Aragonès, D. Aravena, J. I. Cerdá, Z. Acís-Castillo, H. Li, J. A. Real, F. Sanz, J. Hihath, E. Ruiz and I. Díez-Pérez, *Nano Lett.*, 2016, **16**, 218–226.
45 K.-N. Shih, M.-J. Huang, H.-C. Lu, M.-D. Fu, C.-K. Kuo, G.-C. Huang, G.-H. Lee, C. Chen and S.-M. Peng, *Chem. Commun.*, 2010, **46**, 1338.
46 C. Yang, I. P. Liu, Y. Hsu, G. Lee, C. Chen and S. Peng, *Eur. J. Inorg. Chem.*, 2013, **2013**, 263–268.
47 M. C. Barral, R. González-Prieto, S. Herrero, R. Jiménez-Aparicio, J. L. Priego, E. C. Royer, M. R. Torres and F. A. Urbanos, *Polyhedron*, 2004, **23**, 2637–2644.
48 K. Nakamoto, *Infrared and Raman Spectra of Inorganic and Coordination Compounds: Part B: Applications in Coordination, Organometallic, and Bioinorganic Chemistry*, Wiley, 1st edn, 2008.
49 F. A. Cotton and T. Ren, *Inorg. Chem.*, 1995, **34**, 3190–3193.
50 W.-Z. Chen, F. A. Cotton, N. S. Dalal, C. A. Murillo, C. M. Ramsey, T. Ren and X. Wang, *J. Am. Chem. Soc.*, 2005, **127**, 12691–12696.

51 J. Ying, I. P. Liu, B. Xi, Y. Song, C. Campana, J. Zuo and T. Ren, *Angew. Chem., Int. Ed.*, 2010, **49**, 954–957.
52 F. C. Simeone, H. J. Yoon, M. M. Thuo, J. R. Barber, B. Smith and G. M. Whitesides, *J. Am. Chem. Soc.*, 2013, **135**, 18131–18144.
53 C. M. Bowers, D. Rappoport, M. Baghbanzadeh, F. C. Simeone, K.-C. Liao, S. N. Semenov, T. Żaba, P. Cyganik, A. Aspuru-Guzik and G. M. Whitesides, *J. Phys. Chem. C*, 2016, **120**, 11331–11337.